Available online at www.sciencedirect.com
SCIENCE DIRECT®
Journal of Power Sources 142 (2005) 103–116
JOURNAL OF POWER SOURCES
www.elsevier.com/locate/jpowsour

Characterization and quantification of uncertainty in solid oxide fuel cell hybrid power plants

Karthik Subramanyan, Urmila M. Diwekar*

Center for Uncertain Systems, Tools for Optimization and Management, Departments of Bio and Chemical Engineering, Institute of Environmental Science and Policy, 851 S. Morgan Street, University of Illinois at Chicago, Mail Code 063, Chicago, IL 60607, USA

Received 16 August 2004; accepted 10 September 2004
Available online 21 January 2005

Abstract

Distributed power generation is one of the most powerful applications of fuel cell technology. Several types of configurations have been hypothesized and tested for these kinds of applications at the conceptual level, but hybrid power plants are one of the most efficient. These are designs that combine the fuel cell cycle with other thermodynamic cycles to provide higher efficiency. The power plant in focus is the high pressure (HP)–low pressure (LP) solid oxide fuel cells (SOFC)/steam turbine (ST)/gas turbine (GT) configuration which is a part of the vision-21 program, which is a new approach, the U.S. Department of Energy's (DOE's) Office of Fossil Energy has begun, for developing 21st century energy plants that would have virtually no environmental impact. The overall goal is to effectively eliminate—at competitive costs—environmental concerns associated with the use of fossil fuels, for producing electricity and transportation fuels. In this design, coal is gasified in an entrained bed gasifier and the syn-gas produced is cleaned in a transport bed desulfurizer and passed over to cascaded SOFC modules (at two pressure levels). This module is integrated with a reheat GT cycle. The heat of the exhaust from the GT cycle is used to convert water to steam, which is eventually used in a steam bottoming cycle. Since this hybrid technology is new and futuristic, the system level models used for predicting the fuel cells' performance and for other modules like the desulfurizer have significant uncertainties in them. Also, the performance curves of the SOFC would differ depending on the materials used for the anode, cathode and electrolyte. The accurate characterization and quantification of these uncertainties is crucial for the validity of the model predictions and hence is the main focus of this paper. This work performs a two-level uncertainty analysis of the fuel cell module: uncertainty associated with (1) model and (2) material used for anode, cathode and electrolytes. Following that the paper deals with the uncertainty analysis of the desulfurization reaction module based in particular on the activation energy and frequency factors for different sorbents used. This paper lays the basis for two analyses: (1) the effect of uncertainties on the trade-off surface obtained through a multi-objective optimization framework; (2) development of the "value of research" framework which is concerned with analyzing the trade-offs between allocation of resources for the reduction of uncertainties and benefits accrued to the objectives through this reduction [K. Subramanyan, U. Diwekar, The 'value of research' methodology applied to the solid oxide fuel cell/steam turbine/gas turbine hybrid power plant design, Ind. Eng. Chem. Res., submitted for publication].

Keywords: Distributed generation; Hybrid power plant; Uncertainty; Characterization; Quantification

1. Introduction

Uncertainties are inherent in life and most of us have learnt to deal with them by evolving cognitive heuristics and developed strategies. However, as the system becomes complicated, involving more decisions and much higher stakes, heuristics becomes obsolete and mathematical models are required. This paper deals with scientific and technical uncertainties in policy-focused research, more particularly, with the uncertainties inherent in the high pressure–low pressure (HP–LP)SOFC/steam turbine (ST)/gas turbine (GT) hybrid

* Corresponding author. Tel.: +1 312 355 3277; fax: +1 312 355 0760.
E-mail address: urmila@uic.edu (U.M. Diwekar).

0378-7753/$ – see front matter © 2004 Elsevier B.V. All rights reserved.
doi:10.1016/j.jpowsour.2004.09.030

power plant with particular emphasis on the solid oxide fuel cell (SOFC) and desulfurization (DESU). The reason for designating the research as "policy-focused" is because the uncertainty analysis is used in developing the "*value of research*" methodology which assesses the trade-offs between allocation of resources for uncertainty reduction and the benefits accrued to the objectives through this reduction. This gives us an idea of how much weight should be given to uncertainty research. For more details on this methodology, refer to [1]. Until recently, these types of uncertainties have been treated in much the same way we have dealt with other uncertainties in our private and public lives. However, the past decade has seen a growing recognition that policies that ignore uncertainty about technology often lead to unsatisfactory technical and social outcomes [2]. For example, uncertainties in the fuel cell models were found to have a considerable impact on the optimal designs of the solid oxide fuel cell–proton exchange membrane hybrid power plant [3].

This paper, dealing with the uncertainties in the SOFC and desulfurization modules, is an off-shoot of our major research concerning simulation and optimization of the design and performance of the (HP–LP)SOFC/ST/GT hybrid power plant which consists of cascaded SOFC at two pressure levels integrated with a reheat GT cycle and a steam bottoming cycle [4]. This plant belongs to the vision-21 power plants program [5,6] initiated by the U.S. Department of Energy (DOE). During the course of our research, we identified that a large number of materials were needed to be considered in the fuel cells for electrolyte issues, electrode performance issues, and for different configurations, in order to obtain the desired properties. Also, since the hybrid power plant is new technology, the models developed to simulate the SOFC are not exact. Further, the development in the area of new materials and other technologies where the performance and economic data are scarce and/or incomplete calls for consideration of uncertainties in the design and optimization. The performance of the desulfurization module also varies depending on the sorbent used for the absorption. Hence, the accurate characterization and quantification of these uncertainties play a crucial role in the proper simulation of the plant and accurate prediction of objectives. This paper details the process of characterization and quantification of uncertainties in the SOFC and desulfurization modules of the SOFC/ST/GT hybrid power plant.

The section following this introduction gives a brief overview of the SOFC/ST/GT hybrid power plant conceptual design. In the course of description of the plant, the section also describes in detail the operation of the SOFC and the models developed for the SOFC and desulfurizer used in the simulation. Section 3 discusses the quantification and characterization of uncertainty in the SOFC and in the desulfurization module in detail. Section 4 presents the effect of uncertainties on the minimum cost design. The final section puts forth conclusions drawn from this work.

2. Solid oxide fuel cell/steam turbine/gas turbine hybrid power plant conceptual design

This section explains the structure of each individual section of the SOFC/ST/GT hybrid power plant briefly. Fig. 1 shows the Aspen flowsheet for this vision-21 power plant.

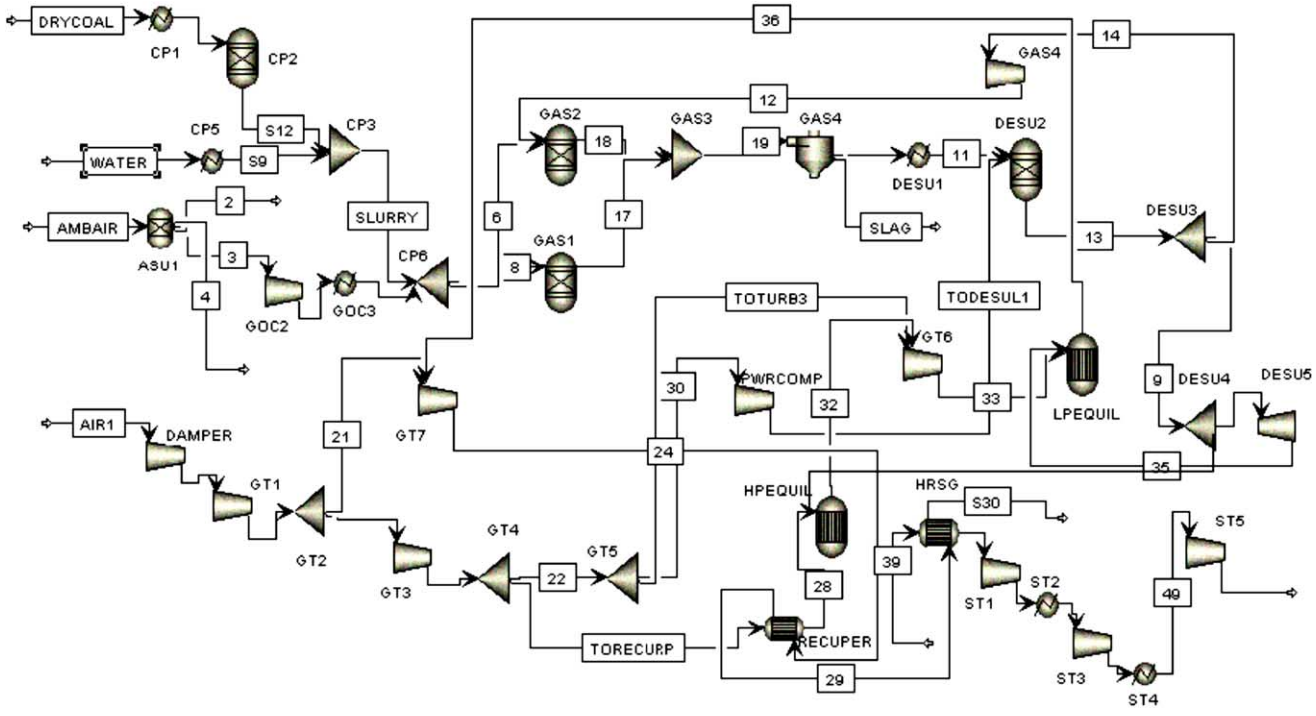

Fig. 1. Aspen flowsheet for the vision-21 (HP–LP)SOFC/ST/GT hybrid power plant.

Only the major blocks have been shown in the flowsheet and the abbreviation of each section is attached to the respective block.

2.1. Air separation unit (ASU)

The purpose of this module is to separate O_2 and N_2 in ambient air (AMBAIR), since the gasifier (GAS) requires a pure oxygen stream. Ambient air (O_2, 21%; N_2, 79%) enters the air separation unit and is split into three streams: stream 3—95% of oxygen to the gasifier, stream 4—100% N_2 and stream 2—rest to the molecular sieve vent.

2.2. Gasifier oxidant compressor (GOC)

The oxygen stream from the ASU at ambient conditions is compressed using an isentropic compressor and heated for better gasification performance.

2.3. Coal preparation (CP)

The dry coal is crushed and mixed with water in a hopper resulting in coal slurry with 60% by weight of solids and is passed to the gasifier.

2.4. Entrained-bed gasifier

The coal slurry and O_2 streams enter the entrained-bed gasifier. Approximately 78% of the total slurry feed is gasified/combusted in the first (lower) stage (GAS1). Highly exothermic reactions occur that result in temperatures of 2400–2600 °F. In the upper vertical cylindrical stage (GAS2), the remaining coal slurry is fed and additional gasification occurs.

2.5. Desulfurization module

The syn-gas produced during gasification contains prohibitive amounts of hydrogen sulfide (H_2S) which has to be removed if the plant is to abide by emission standards. The transport desulfurizer model used in our simulation is based on the work on hot-gas transport desulfurizer by Luyben and Yi [7,8]. Transport reactors can be operated at higher gas velocity, which leads to smaller diameter vessels and hence lower capital cost. They have the additional advantage of providing better solid/gas contact, so less solid hold-up is required.

2.5.1. Brief overview of the model

There are assumed to be seven perfectly mixed zones arranged in series in the axial direction. These solid zones

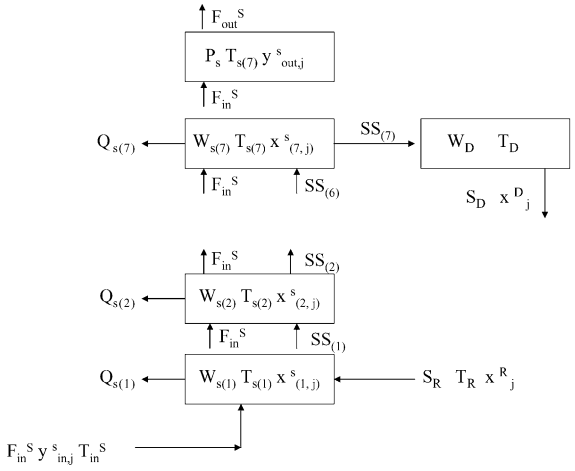

Nomenclature:

$Q_{s(i)}$: Heat removed from ith zone in desulfurizer (Kj/hr); T^s_{in}: Temp.of inlet syn-gas to desulf. (deg.C)
$y^s_{in,j}$: mole fr. of jth component in inlet gas to desulf; F^s_{in}: Mole flow of inlet syn-gas to desulf (kgmol/hr)
$W_{s(i)}$: solids hold-up in ith zone in desulf. (kg); F^s_{out}: Mole flow of outlet syn-gas from desulf (kgmol/hr)
$T_{s(i)}$: Temp. of ith zone in desulf. (°C); $y^s_{out,j}$: mole fr. of jth component in inlet gas to desulf;
$x^s_{i,j}$:mole fr. of jth component of solid in ith zone in desulf; W_D: solids hold-up in drum (kg)
SS_i: solid flowrate from ith zone in desulf (kg/hr); x^D_j: mole fr. of jth component of solid in drum
T_D: Temp. in drum (°C); S_R: Solids flowrate from regen. to desulf. (kg/hr)
S_D: solid flow rate from drum (kg/hr); T_R: Temp. in regenerator (°C);
x^D_j: mole fr. of jth component of solid in regenerator

Fig. 2. Schematic of the desulfurizer model used in the SOFC/ST/GT simulation.

have different solid hold-ups, solid compositions and temperatures. The gas flows up through these seven zones in series in plug-flow. There are only two phases in the bed: rising gas and solid. Mass transfer and reaction are lumped together by calculating the conversion of H_2S or the production of sulfur dioxide (SO_2) from a reaction rate that assumes first-order dependence on the concentration of the reactant in the gas and the concentration of MeO or MeS in the solid. The reactions that occur in the desulfurizer and regenerator are:

$$\text{Sulfidation reaction : MeO} + H_2S \rightarrow \text{MeS} + H_2O$$

$$\text{Regeneration reaction : MeS} + 1.5O_2 \rightarrow \text{MeO} + SO_2$$

Due to the small mass of gas in the system, the dynamics of the gas phase are much faster than those of the solid phase leading to ordinary differential equations for the gas concentration in each zone with bed height as the independent variable. This can be analytically integrated to yield an algebraic equation for the concentration of the gas-phase leaving the top of each of the seven beds at each point in time. A schematic of the model is shown in Fig. 2.

2.5.2. Model validation

The results obtained from our model were compared with those given in Luyben and Yi [7,8] and there was a perfect match. For example, the temperature of the outlet gas is given as 550 °C in their paper [7,8] which is exactly what has been obtained by integration of the model differential equations by LSODE [9] package as shown in Fig. 3. For the complete model equations and code of the model, refer to appendices C and G, respectively, of reference [10].

When the model was scaled up to the vision-21 hybrid power plant specifications, there were four unknown parameters: (1) mass flow rate of sorbent to the desulfurizer (SRI, $kg\,h^{-1}$); (2) molar flow rate of oxygen to the regenerator (FINRI, $kg\,mol\,h^{-1}$); (3) total heat removed from the desulfurizer (QSI, $kJ\,h^{-1}$); (4) total heat removed from regenerator (QRI, $kJ\,h^{-1}$). These parameters were calculated using an optimization block, with minimum H_2S as the objective. The optimization problem set up is given in Table 1.

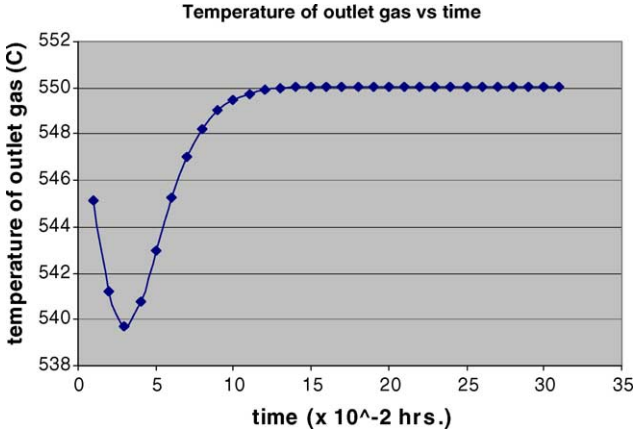

Fig. 3. Results of integration with LSODE for temperature of outlet gas.

Table 1
Optimization problem set up for the minimization of H_2S

Objective
Minimize "H_2S"
Decision variables
Vary SRI → limits "92 000"–"110 000"
Vary FINRI → limits "35 000"–"50 000"
Vary QSI → limits "184 400"–"204 000"
Vary QRI → limits "184 400"–"204 000"
Constraints
Mole fraction of all components >0 and <1

2.6. High pressure and low pressure solid oxide fuel cells

The desulfurized syn-gas is split and one part is recycled back to the gasifier after compression. The other part is divided between the HP and LPSOFC which are at pressures of 15 and 3 atm, respectively. The syn-gas is expanded before entering the LPSOFC.

2.6.1. Description of an SOFC

The basic physical structure or building block of a SOFC or for any fuel cell consists of an electrolyte layer in contact with a porous anode and cathode on either side. The fuel or oxidant gases flow past the surface of the anode or cathode opposite the electrolyte and generate electrical energy by the electrochemical oxidation of fuel, usually hydrogen, and the electrochemical reduction of the oxidant, usually oxygen. The electrolyte not only transports dissolved reactants to the electrode, but also conducts ionic charge between the electrodes and thereby completes the cell electric circuit. The functions of porous electrodes in fuel cells are to provide a surface site where gas/liquid ionization can take place and to conduct ions away from interface once they are formed.

Fig. 4 shows the operating principle of a SOFC. The electrochemical reactions occurring in SOFC utilizing H_2 and O_2 are based on Eqs. (2.1) and (2.2) [11].

At the *anode*:

$$H_2 + O^{2-} \rightarrow H_2O + 2e^- \tag{2.1}$$

At the *cathode*:

$$\frac{1}{2}O_2 + 2e^- \rightarrow O^{2-} \tag{2.2}$$

The overall cell reaction:

$$H_2 + \frac{1}{2}O_2 \rightarrow H_2O \tag{2.3}$$

Solid oxide fuel cells have grown in recognition as a viable high-temperature fuel cell technology due to several characteristics:

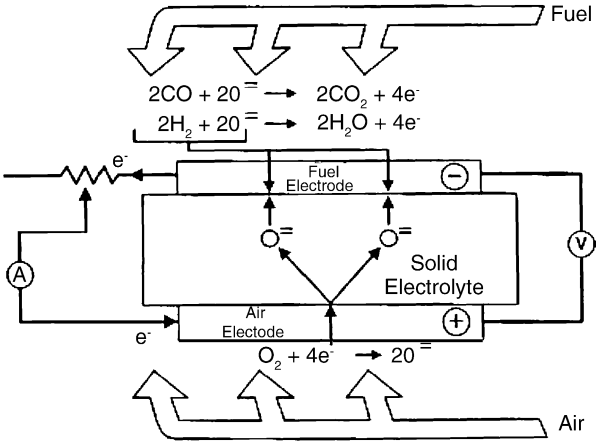

Fig. 4. Operating principle of a SOFC.

- SOFC can use CO as a fuel and is relatively more tolerant of impurities like sulfur than other conventional fuel cells. This leads to the ability to use a variety of hydrocarbon fuels with simpler reforming processes.
- There is no need for noble or precious metals as catalysts which leads to greater cost-effectiveness (even if the manufacturing process is quite complex).
- The electrolyte is dry and so the humidification of the reactants is not necessary and no water management system is required.
- The operating temperature greater than 800 °C allows internal reforming, promotes rapid kinetics with non-precious materials, and produces high-quality byproduct heat for cogeneration or for use in a bottoming cycle which makes it ideal for hybrid power plant balance of plant subsystems.

As with batteries, individual fuel cells must be combined to produce appreciable power levels and so are joined in series by interconnects in a stack. Interconnects must be electrical conductors and impermeable to gases. Fig. 5 shows a schematic stack configuration of a planar solid oxide fuel cell.

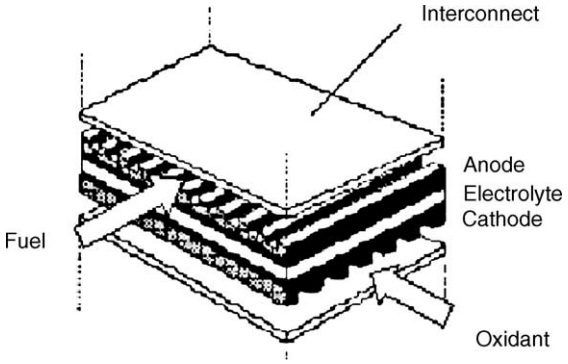

Fig. 5. Schematic of an SOFC stack.

2.6.2. SOFC models

The SOFC/ST/GT hybrid power plant was modeled using Aspen Plus [12] simulation software. Since the software does not include any inbuilt fuel cell model, two approaches were taken to overcome this problem. The first way was to use a standard reactor model, like a stoichiometric and/or equilibrium reactor, to perform energy and mass balances around the fuel cell. This unit was to be then coupled with a polarization model for voltage and current computations. Alternatively, a new unit (User Model) based on a FORTRAN subroutine could be used to perform mass and energy balances and polarization characterization. The former method was used to model the HPSOFC and LPSOFC modules.

The methodology that was used to simulate the SOFC stack for impact assessment is similar to the one utilized by Geisbrecht [13]. An equilibrium reactor at fixed temperature performs heat and material balances on the cell and then, after flowsheet convergence, an Aspen calculator block computes voltage, current density and total cell area applying a polarization model.

The reactions that take place in a fuel cell are: methane steam reforming, carbon monoxide water shift and hydrogen electrochemical oxidation.

$$CH_4 + H_2O \rightleftarrows 3H_2 + CO \text{ (methane steam reforming)}$$

$$CO + H_2O \rightleftarrows CO_2 + H_2 \text{ (CO water shift)}$$

$$H_2 + \frac{1}{2}O_2 \rightarrow H_2O \quad \text{(electrochemical oxidation)}$$

The first two reactions are at equilibrium [14] while hydrogen oxidation has fixed extent in order to match the given fuel utilization. Fuel utilization is defined as:

$$U_f = \frac{H_2^{reacted}}{4CH_4^{in} + CO^{in} + H_2^{in}} \tag{2.4}$$

where $H_2^{reacted}$ are the total moles of hydrogen reacted; CH_4^{in}, CO^{in}, H_2^{in} the moles of methane, carbon monoxide and hydrogen entering the cell; '4' the moles of H_2 generated by each mole of methane; and '1' is the mole of H_2 generated by each mole of CO.

The reaction extent of the electrochemical reaction is determined by a "design specification" that acts as a feedback controller. Reaction extent is manipulated so that:

$$O_2^{in} - O_2^{out} = \frac{1}{2}U_f(4CH_4^{in} + CO^{in} + H_2^{in}) \tag{2.5}$$

where O_2^{in} and O_2^{out} are the moles of oxygen entering and exiting the cell and U_f is the fuel utilization. Oxygen was chosen as reference element because it reacts only with hydrogen. Recycling of the gaseous outlet of the cell is necessary in order to reach the desired fuel conversion. The electrochemical oxidation of CO was neglected because in presence of water, the favorable path for the oxidation of carbon monoxide is generating hydrogen by the water shift reaction [11,14].

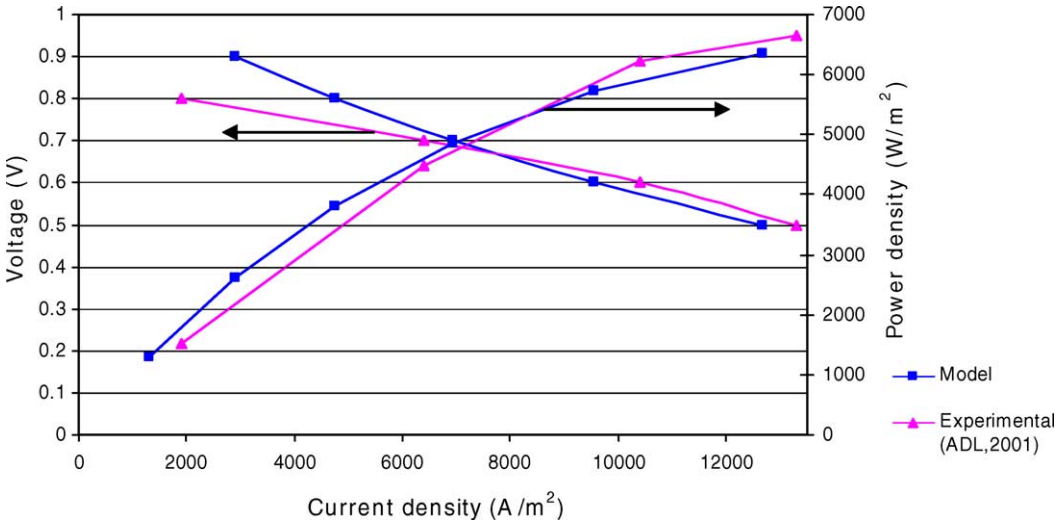

Fig. 6. Comparison between model and experimental data.

At fixed temperature, a heat balance around the reactor gives the power output of the cell. The power output divided by the current (known once the fuel utilization is fixed) gives the voltage of the cell. Current can be computed as

$$I = 2F\mathrm{H}_2^{\mathrm{reacted}} = 2FU_{\mathrm{f}}(4\mathrm{CH}_4^{\mathrm{in}} + \mathrm{CO}^{\mathrm{in}} + \mathrm{H}_2^{\mathrm{in}}) \quad (2.6)$$

where I is the current and F is the Faraday constant (96 485 C mol^{-1}).

At this point, an SOFC polarization model is used to find the current density of the cell at that given voltage.

There are number of papers in the literature concerning SOFC behavior modeling. As a first step, they can be classified as steady state [15–22] and dynamic [23] models. A one-dimensional, steady state, algebraic polarization model derived from literature [17] was used for our study. This particular model was chosen because of its simplicity and comprehensive nature (applicability to every operating condition and sensitivity to the various design components of the cell). Overpotential equations, based on the complete Butler–Volmer and diffusion equations, are obtained together with the necessary parameters from the reference [17].

Since the model gives the voltage as a function of current density, Newton method (Eqn. 2.8) was applied in order to obtain iteratively the current density at the desired voltage:

$$V(i) - \bar{V} = f(i) = 0 \quad (2.7)$$

$$i_{n+1} = i_n - \alpha\frac{f(i)}{f'(i)} \quad (2.8)$$

where $V(i)$ is the voltage as function of current density (i), $\bar{V}$ the desired voltage, α a weight parameter, and $f'(i)$ is the numerical derivative of $f(i)$. For the complete code, refer to appendix A of reference [24].

This polarization model was tested with experimental results from reference [25]. Even if the original cell parameters from reference [17] were kept (since no data were provided in reference [25]), the fitting between the model and the experimental data is acceptable for our level of details. The results are shown in Fig. 6.

Once the current density is obtained, current divided by current density gives the total cell area (area of the electrodes), important for cost estimations.

2.7. Gas turbine cycle

The cascaded HP and LPSOFC are integrated with the reheat gas turbine cycle which consists of two air compressors and two expanders. The GT cycle produces a power of around 130 MW.

2.8. Steam turbine cycle

The heat of the exhaust from the SOFCs is used to convert water to steam in a heat recovery steam generator (HRSG) which is used in a steam bottoming cycle to produce around 118 MW of power.

Table 2 gives the distribution of power output between various sections of the power plant.

3. Characterization and quantification of uncertainty

The process of uncertainty analysis consists of four main steps: (1) characterization and quantification of uncertainty,

Table 2
Distribution of power output between various sections of the power plant

System performance summary	
Gas-turbine cycle power output (MW)	133.67
Steam-turbine cycle (MW)	110.05
HPSOFC (MW)	188
LPSOFC (MW)	112
Gross power (MW)	560
Auxiliary power consumption (MW)	40
Net power (MW)	520

(2) sampling, (3) propagation through framework, (4) analysis of results. The first step is of foremost importance on which the validity of the uncertainty analysis rests on. Characterization refers to the process of representing uncertainty through mathematical expressions in order to facilitate analysis with mathematical tools. Quantification refers to the representation of uncertainty with probability distribution functions (PDF) which illustrate the frequency of occurrence of each uncertainty. In uncertainty analysis, variables which are functions of the uncertain parameters do not have a specific point value. They are represented as expected values over repeated iterations. The probability distributions of each uncertain parameter is sampled and propagated through the framework. This is repeated a specific number of times to compute the expected value of the objectives. The sampling technique employed also has an impact on the uncertainty analysis. However, that discussion is beyond the scope of this paper.

3.1. Uncertainty in the SOFC

The hybrid fuel cell technologies are new and futuristic and hence the system level models used to estimate the SOFCs' performance have significant uncertainties in them. Also, the performance curves of the SOFCs would differ depending on the materials for the anode, cathode and electrolyte.

A two-level uncertainty analysis was performed for the SOFC modules. Performance data, i.e. current density (I) versus voltage (V) data, for SOFC were collected from literature [26–70] and two types of uncertainties were identified:

- *model uncertainty*: uncertainty in the parameters used in the SOFC model;
- *material induced uncertainty*: uncertainty due to the various materials used for anode, cathode and electrolyte in the SOFCs resulting in different performance curves.

In order to differentiate between these two types of uncertainties, data for various anode, cathode and electrolyte materials were collected from literature. This involved digitizing the experimental graphs to obtain the actual numbers, resulting in I versus V experimental data for 45 materials. To calculate the uncertainty factor (UF), we required the voltage calculated using the SOFC model. This called for estimation of some missing parameters using non-linear programming (NLP) optimization (minimization of square of error) technique and eventually, the voltage was calculated using the SOFC model which computes cell voltage as a function of current density. Thereby, we obtained voltage values at the current densities matching our experimental data. For the code developed for this parameter estimation process, refer to appendix B of reference [10]. Using this I versus V_{expt} and

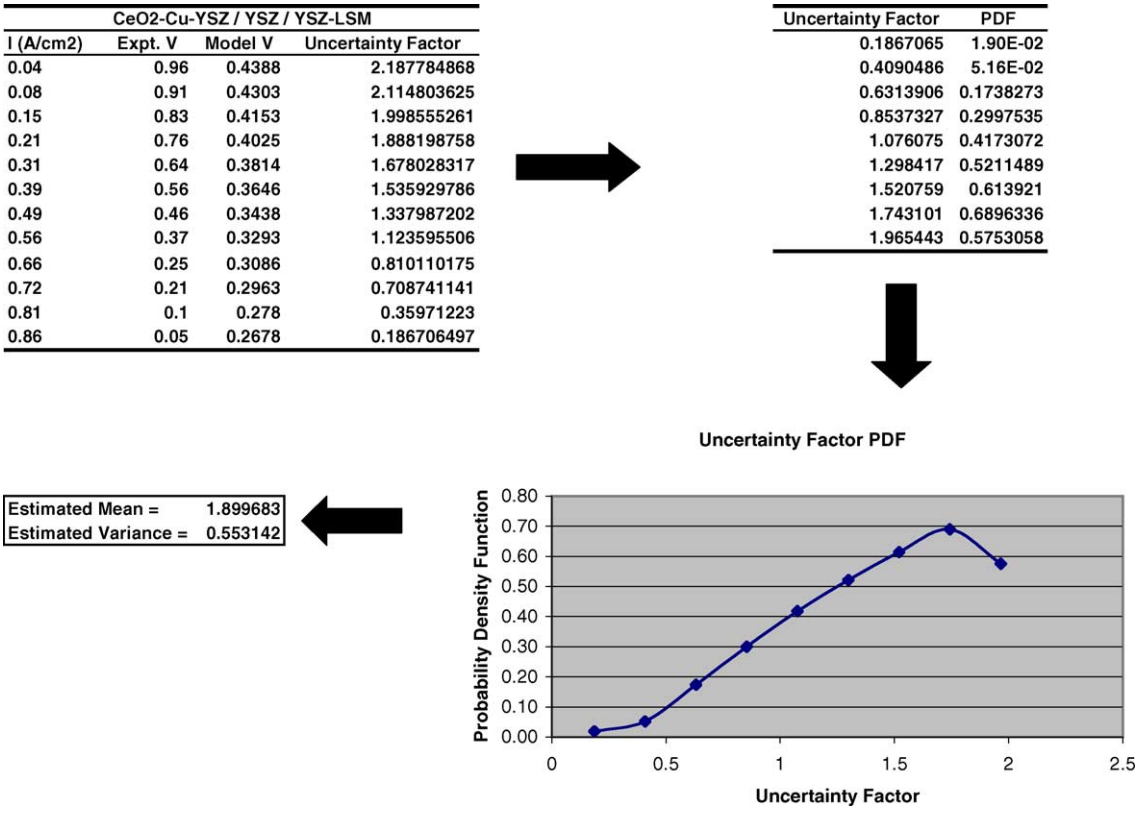

Fig. 7. Schematic of the process of computing UF distribution, mean and variance for a particular anode/electrolyte/cathode material set.

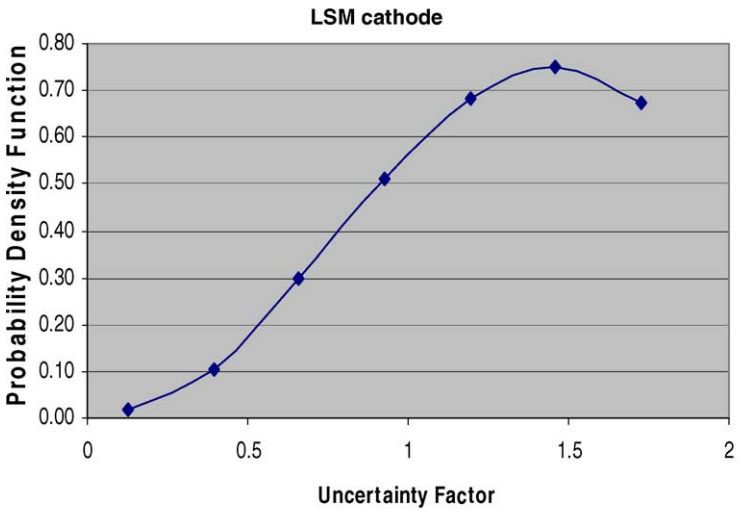

LSM cathode at 700 deg C			
I	V(expt)	V(model)	
A/cm^2	Volts	Volts	
x	y (expt)	y(model)	UF
0.02	0.9	0.442	2.036199
0.04	0.8	0.4388	1.823154
0.1	0.7	0.4292	1.630941
0.17	0.6	0.4182	1.43472
0.22	0.53	0.4105	1.291108
0.26	0.47	0.4043	1.162503
0.42	0.36	0.3802	0.94687
0.47	0.3	0.3728	0.804721
0.55	0.24	0.3612	0.664452
0.66	0.15	0.3454	0.434279
0.74	0.09	0.3341	0.26938
0.81	0.04	0.3244	0.123305

Mean = 1.58 Variance = 0.99

Fig. 8. The estimated UF distribution mean and variance for LSM cathode material and base anode and electrolyte materials are CeO_2–Cu–YSZ and YSZ, respectively.

I versus V_{model} data, $UF_{mat,i}$ was defined as:

$$UF_{mat,\,i} = \frac{\text{experimental voltage for } i\text{th material}}{\text{model calculated voltage for } i\text{th material}} \quad (3.1)$$

By this process, UF_{mat} distribution is obtained for each anode/electrolyte/cathode material set. The schematic for computing the UF_{mat} for a particular cathode/anode/electrolyte combination is given in Fig. 7. The results of applying the same methodology on two other cathode and anode materials are given in Figs. 8 and 9, respectively. When the methodology was applied to all 45 materials, it was found that for majority of the materials, the UF distribution was log-normal. Using the log-normal probability density function, mean and variance equations shown in Eqs. (3.3)–(3.5) [71], the moments for each distribution are estimated. Through this, we obtained mean ($UF_{mat,mean,i}$) and variance ($UF_{mat,var,i}$) values for 45 materials shown in Table 3. The following are the abbreviations in Table 3: GDC—$Ce_{0.9}Gd_{0.1}O_{1.95}$; SSC—$Sm_{0.5}Sr_{0.5}CoO_3$; ZYO—$Zr_{0.84}Y_{0.16}O_{1.92}$; LSM—$La_{0.85}Sr_{0.15}Mn_{1.1}O_3$; LSGMC1—

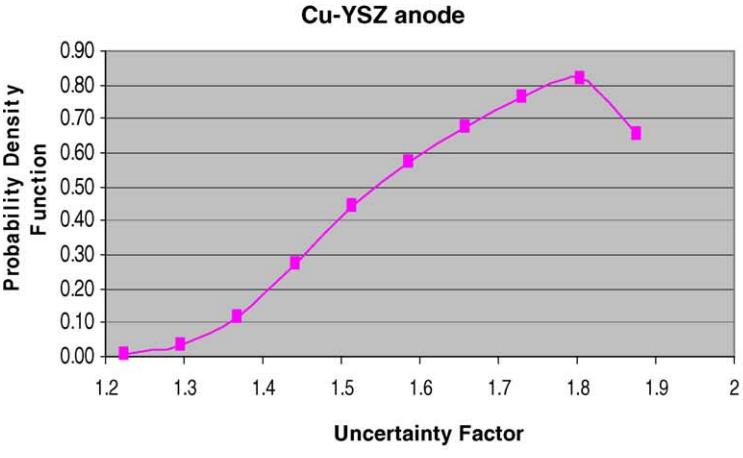

Cu p-YSZ at 700 deg C			
I	V(expt)	V(model)	
A/cm^2	Volts	Volts	
x	y (expt)	y(model)	UF
0.04	0.84	0.3867	2.172227
0.06	0.75	0.3796	1.975764
0.08	0.7	0.3726	1.87869
0.09	0.61	0.3691	1.652669
0.11	0.52	0.3623	1.435275
0.12	0.45	0.3589	1.253831
0.14	0.38	0.3522	1.078932
0.15	0.31	0.3489	0.888507
0.17	0.21	0.3423	0.613497
0.19	0.14	0.3359	0.416791
0.2	0.07	0.3327	0.2104
0.21	0.03	0.3295	0.091047

Mean= 1.82; Variance = 1.41

Fig. 9. The estimated UF distribution mean and variance for Cu–YSZ anode material and base cathode and electrolyte materials are YSZ–LSM and YSZ, respectively.

Table 3
Type of distribution, mean and variance of UF distributions for all anode/electrolyte/cathode materials

Anode/electrolyte/cathode assembly	Distribution	Mean	Variance
$La_{0.6}Sr_{0.4}Fe_{0.8}Co_{0.2}O_{3-x}$/YSZ/LSM	Log-normal	1.62	0.43
Ni + GDC/SSC + 10 wt.% GDC/GDC	Log-normal	1.71	0.0335
$Sr_{0.2}Ba_{0.4}Ti_{0.2}Nb_{0.8}O_3$/YSZ–$Al_2O_3$/Pt	Log-normal	1.96	1.11
$SrCo_{0.8}Fe_{0.2}O_{3-x}$/YSZ/LSM	Log-normal	1.88	1.04
Ni–8YSZ/TZ3Y/Sr doped $LaMnO_3$	Log-normal	1.92	0.038
$SrFeCo_{0.5}O_x$/YSZ/LSM	Log-normal	1.84	0.65
Ni-50 wt.% GDC/GDC/SSC	Log-normal	1.57	0.068
SYTG/ZYO/$SrTiO_3$	Log-normal	1.57	0.29
Ni–YSZ/YSZ/LSM	Log-normal	1.91	0.71
Cu p-YSZ/YSZ/LSM	Log-normal	1.82	1.41
CeO_2–Cu p-YSZ/YSZ/LSM	Log-normal	1.58	0.99
LSFC/YSZ/LSM + 20 wt.%YSZ	Log-normal	1.79	1.08
Platinum/ceria/perkovsite	Log-normal	1.96	0.33
Ni–YSZ/20 wt.% of $Ce_{0.8}Gd_{0.2}O_{1.9}$/LSM	Log-normal	1.77	0.042
Ni–YSZ/YSZ/10 times SDC coated LSM	Log-normal	1.71	0.21
Ni–YSZ/YSZ/(LSM1–$MnCO_3$)–(YSZ)	Log-normal	2.12	0.04
Ni–YSZ/YSZ/10 times (YSZ) coated LSM	Log-normal	1.63	0.20
SDC/YSZ/$La_{0.85}Sr_{0.15}MnO_3$	Log-normal	1.28	0.031
Ni–YSZ/YSZ/(LSM1) (40 vol.%)–(YSZ)	Log-normal	1.61	0.41
Ni–YSZ/CGO/60 wt.% of $Ce_{0.8}Gd_{0.2}O_{1.9}$	Log-normal	1.77	0.32
Ni–YSZ/CGO/30 wt.% of $Ce_{0.8}Gd_{0.2}O_{1.9}$	Log-normal	1.73	0.34
Ni–YSZ/CGO/10 wt.% of $Ce_{0.8}Gd_{0.2}O_{1.9}$	Log-normal	1.76	0.38
Ni–YSZ/CGO/0 wt.% of $Ce_{0.8}Gd_{0.2}O_{1.9}$	Log-normal	1.89	0.68
LSM–YSZ/YSZ/YSZ	Log-normal	1.60	0.89
LSM–YSZ/YSZ/gadolinia doped ceria	Log-normal	1.41	0.35
Ni–YSZ/CGO/LSM1 [5 wt.% C powder]	Log-normal	1.39	0.88
Ni–YSZ/CGO/LSM2 [0 wt.% C powder]	Log-normal	1.57	0.065
Ni–YSZ/CGO/LSM3 [10 wt.% C powder]	Log-normal	1.55	0.022
Ni–YSZ/YSZ/(LSM1) (50 vol.%)–(YSZ)	Log-normal	1.65	0.62
Ni–ceria/$La_{0.6}Sr_{0.4}Co_{0.2}Fe_{0.8}O_3$/LSGM	Log-normal	1.85	0.10
NiO–CLO/CLO/lithiated Ni–CLO	Log-normal	2.26	0.91
Pt/Sr-doped $LaInO_3$/Pt	Log-normal	1.48	0.40
Pt/Sr $Ce_{0.95}Yb_{0.05}O_3$/Pt	Log-normal	2.29	0.36
CGO–LSM/CGO–LSM/LSM–(YSZ)	Log-normal	1.22	0.24
Pt/LSGM/Pt	Log-normal	1.82	0.14
Pt/doubly doped ceria/Pt	Log-normal	2.09	0.89
LSFC/GDC/Ni–YSZ	Log-normal	1.75	0.21
Ni–CeO_2/LSGMC1/SSC	Log-normal	1.56	0.36
Ni–CeO_2/LSGMC2/SSC	Log-normal	2.19	2.09
CeO_2–Cu–YSZ/YSZ/YSZ–LSM	Log-normal	1.89	0.55

$La_{0.8}Sr_{0.2}Ga_{0.8}Mg_{0.15}Co_{0.05}O_{3-x}$; CLO—$CeO_2$–$La_2O_3$; LSGMC2—$La_{0.8}Sr_{0.2}Ga_{0.8}Mg_{0.115}Co_{0.085}O_3$; LSGM—$La_{0.9}Sr_{0.1}Ga_{0.8}Mg_{0.2}O_{2.85}$; CGO—gadolinium doped ceria; LSFC—$La_{0.6}Sr_{0.4}Co_{0.2}Fe_{0.8}O_3$; SDC—$Sm_{0.2}Ce_{0.8}O_2$; YSZ—yittirium-stabilized zirconia; SYTG—$Sr_{0.85}Y_{0.10}Ga_{0.05}O_{3-x}$.

It can be noted from Figs. 8 and 9 and Table 3 that estimated mean and variance for different anode/electrolyte/cathode combination materials are different. This phenomenon is due to the uncertainty associated with the materials. The total mean for all the materials which represents the entire uncertainty associated with material selection is calculated by the equation:

$$\mathrm{UF}_{\mathrm{mat,mean},T} = \frac{\sum_{i=1}^{N} \mathrm{UF}_{\mathrm{mat,mean},i}}{N} \tag{3.2}$$

where $\mathrm{UF}_{\mathrm{mat,mean},i}$ is the mean of the UF distribution for the ith anode/electrolyte/cathode material combination; $\mathrm{UF}_{\mathrm{mat,mean},T}$ the total mean of all the individual material UF means; 'N' is the number of anode/electrolyte/cathode materials which in this case is 45.

Log-normal distribution

Probability density function :

$$f(y) = \frac{1}{y\sigma\sqrt{2\Pi}} \exp\left\{\frac{-(\ln y - \mu)^2}{2\sigma^2}\right\}, \quad y > 0 \tag{3.3}$$

Mean : $$E(y) = \exp\left(\mu + \frac{\sigma^2}{2}\right) \tag{3.4}$$

Variance : $$V(y) = \exp(2\mu + \sigma^2)[\exp(\sigma^2) - 1] \tag{3.5}$$

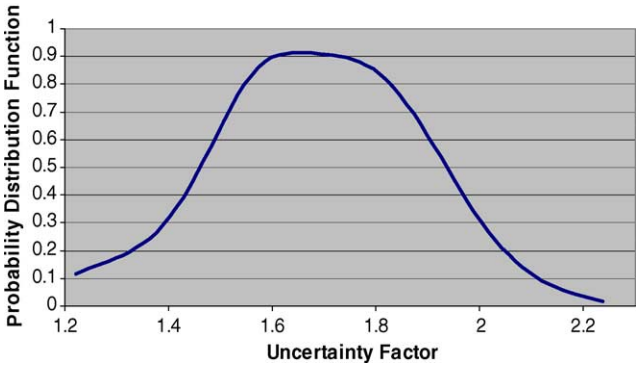

Fig. 10. Combined $UF_{mat,mean}$ distribution for fuel cell materials.

For the model code based on non-linear programming technique [72] developed for the estimation of the mean and variance of each of the given PDFs using Eqs. (3.3)–(3.5) for the log-normal distribution [71], refer to appendix E of reference [10].

The combined distribution of means, $UF_{mat,mean}$, and variances, $UF_{mat,var}$, was calculated and it fitted the normal and log-normal distributions given in Figs. 10 and 11, respectively. The mean and variance of the $UF_{mat,mean}$ distribution were estimated and the mean was found to be equal to that calculated by Eq. (3.2). This figure illustrates the entire uncertainty associated with material selection. With this, material uncertainty analysis is complete and we then moved on to model uncertainty analysis.

The 'model uncertainty' is accounted for by taking the experimental I versus V data for a single material, calculating the ratio of experimental to model voltage thereby computing the uncertainty factor ($UF_{mod,mean}$, $UF_{mod,var}$). The UF distribution for a particular material represents the uncertainty associated with purely the model parameters without the 'noise' of material uncertainty. Hence, the I versus V data for a particular material (in this case, LSM + 50 vol.%YSZ cathode, YSZ electrolyte and Ni–YSZ anode) were chosen and the UF_{mod} distribution was computed. The distribution plot of UF_{mod} (uncertainty factor associated with model parameters) chosen for this model uncertainty is given in Fig. 12.

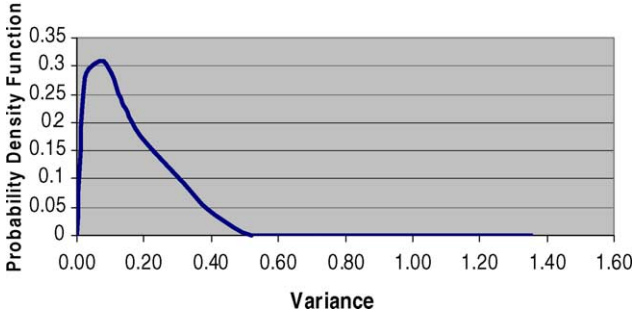

Fig. 11. Combined $UF_{mat,var}$ distribution for fuel cell materials.

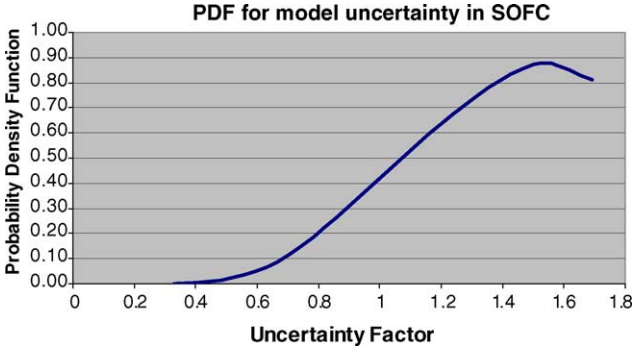

Fig. 12. UF_{mod} distribution for uncertainty in fuel cell model parameters.

3.2. Uncertainty analysis of the desulfurization section

The next step was to deal with the uncertainty associated with the desulfurization reaction [7,8]. The sequential process followed for obtaining uncertainty distribution is:

(1) Desulfurization reaction rate constants (k_s) versus temperature (T) Arrhenius plots ($k_s = k_{s0} \exp(-E_a/RT)$) from literature for different sorbents used in the desulfurization of syn-gas were collected. There was a large amount of literature concerned with removal of sulfur dioxide from the syn-gas. However, our case concerns only hydrogen sulfide removal. Narrowing the literature resulted in Arrhenius plots for 20 different sorbents [73–88].
(2) Each of the plots was digitized to obtain usable k_s versus T data values.
(3) For a particular sorbent, the plot of $1/T$ (K) versus $\ln(k_s)$ gives a linear (or almost linear) curve whose slope is $-E_a/R$ and intercept is $\ln(k_{s0})$.
(4) We obtained k_{s0}—pre-exponential factor and E_a—activation energy values for 20 different sorbents. The first complication was that the k_0 values obtained were of different units and some of them were dependent on the dimensions of the bed. This required obtaining more data related to surface area and density of each sorbent so as to fit out model description. It was found that the difference between various values of these constants was in order of magnitude and hence they had to be scaled by using their logs.
(5) Next we fitted the k_{s0} and E_a values in probability distribution function and both distributions were log-normal.

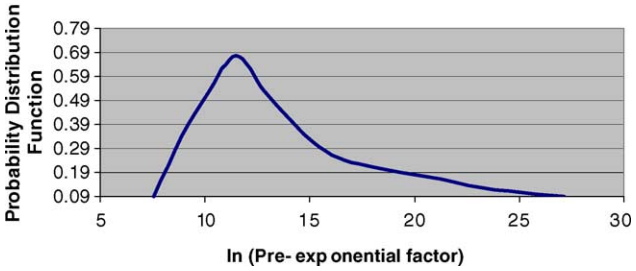

Fig. 13. UF distribution for desulfurization reaction pre-exponential factor.

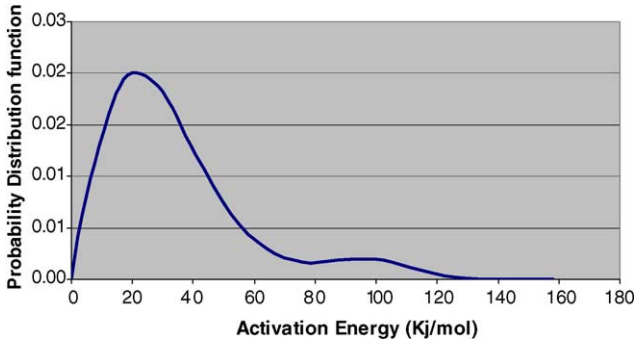

Fig. 14. UF distribution for desulfurization reaction activation energy.

The distribution plots for the desulfurization pre-exponential factor and the activation energy uncertainties are given in Figs. 13 and 14, respectively. From the figures, it can be seen the log of the frequency factors and the activation energy followed log-normal distributions.

With this, the characterization and quantification of uncertainties for the fuel cell module and desulfurization reaction module of the SOFC/ST/GT hybrid power plant was completed. The developed distributions serve two purposes: (1) as mentioned before, they can be used for developing the 'value of research' framework; (2) the fact is that in case of this hybrid power plant, there are multiple objectives like capital cost, CO_2 and SO_2 emissions, etc. to be optimized simultaneously. By sampling the distributions and propagating them through the framework, the effect of uncertainties on the multiple objectives can also be gauged. The following section presents the effect of uncertainties on the minimum cost design.

4. Effect of uncertainties on the minimum cost design

The flowsheet model described earlier is the base case model. We performed optimization to obtain a minimum cost design using sequential quadratic programming (SQP), a non-linear programming technique [72]. The problem formulation describing objective function, constraints and decision variables is presented in Table 4 and the results of the optimization are presented in Fig. 15.

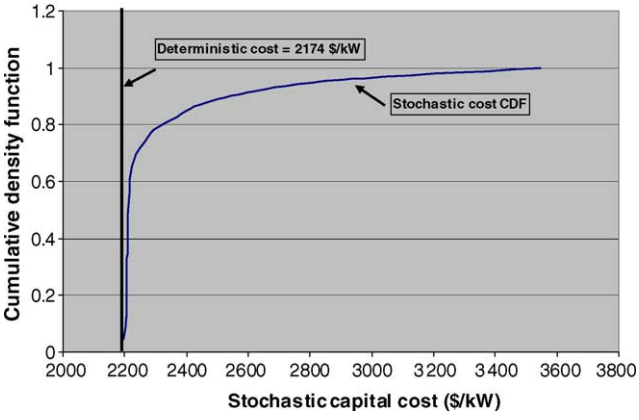

Fig. 15. Comparison of deterministic stochastic capital cost values.

Table 4
The objective, constraints and decision variables for the (HP–LP)SOFC/ST/GT hybrid power plant

Objectives
Minimum capital cost (TCRKW)
Subject to
Mass and energy balance constraints
Power rating of 560 MW (base case)
Decision variables
Fuel utilization (FUT)
Temperature of HPSOFC (HPTEMP)
Temperature of LPSOFC (LPTEMP)
Pressure of HPSOFC (HPPRES)
Split ratio of fuel to HP and LPSOFC (RATIO)
Temperature of fuel inlet to desulfurizer (TRADC)
Mass inlet of dry coal (DRYCOA)

As shown in Table 4, minimum capital cost is the primary objective. The decision variables were identified by performing a sensitivity analysis to identify which input variable had the maximum impact on six different objectives including capital cost. Fig. 15 compares the results of deterministic optimization of the minimum cost design and effect of uncertainties on this minimum cost design. The curve is the cumulative density function of stochastic capital costs and the vertical line is the deterministic capital cost. It is clear from the figure that deterministic optimization has under-predicted the capital cost value significantly. From the figure, it is apparent that there is more than 90% probability that the cost will exceed the deterministic cost. The cost can range from US$ 2174 kW^{-1} to US$ 3547 kW^{-1}.

5. Conclusions

Characterization and quantification are the most important steps in uncertainty analysis on which the accuracy of the whole analysis rests on. This paper dealt with the characterization and quantification of uncertainties in the solid oxide fuel cell and the desulfurization modules for the SOFC/ST/GT hybrid power plant. For the SOFC module, a two-level uncertainty analysis was performed, i.e. both material uncertainty and model uncertainty were considered. The material uncertainty was quantified by: (1) collecting I versus V data for 45 different materials, (2) computing the model voltage for each material, (3) calculating the UF distribution for each material, (4) estimating the mean and variance for each distribution. Finally, distribution of the mean and variance represents the total uncertainty due to materials. The total material-induced distribution was found to be normal with a mean of 1.68. The model uncertainty was calculated by choosing a single material and the distribution was found to be log-normal with a mean of 1.52. This distribution

represented the uncertainty due to the fuel cell model parameters. Next, the uncertainty in the pre-exponential factor and activation energy of the desulfurization reaction was characterized and quantified. The log of frequency factor and activation energy were found to have log-normal distributions with means at 11.5 and 23 kJ mol^{-1}, respectively. The effect of uncertainties on the minimum capital cost design was examined and it was found that deterministic optimization under-predicted the capital cost value significantly.

Acknowledgements

The funding for this work is provided by National Energy Technology Laboratories, NETL/DOE, Morgantown, WV, and the authors thank Francesco Baratto for the SOFC model.

References

[1] K. Subramanyan, U. Diwekar, The 'value of research' methodology applied to the solid oxide fuel cell/steam turbine/gas turbine hybrid power plant design, Ind. Eng. Chem. Res., submitted for publication.
[2] G. Morgan, M. Henrion, A Guide to Dealing with Uncertainty in Quantitative Risk and Policy Analysis, Cambridge University Publishers, 1990.
[3] K. Subramanyan, U. Diwekar, A. Goyal, Multi-objective optimization of hybrid fuel cell power system under uncertainty, J. Power Sources 132 (1–2) (2004) 99–112.
[4] U.S. Department of Energy, Vision 21 Concept Plants: Fuel Cell/Gas Turbine Configuration 1, May 13, 1998.
[5] J.P. Strakey, Vision 21: advanced power plants for the 21st century, in: Presented at the Advanced Coal-based Power and Environmental Systems Conference, July 1998.
[6] http://www.netl.doe.gov/coalpower/vision21/.
[7] W. Luyben, C.K. Yi, Dynamic modeling of a hot gas desulfurization process with a transport desulfurizer, Ind. Eng. Chem. Res. 40 (2001) 1157–1167.
[8] C.K. Yi, W. Luyben, Dynamic model and control structure of a hot gas desulfurization fluidization process, Ind. Eng. Chem. Res. 38 (1999) 4290–4298.
[9] K. Radhakrishnan, A.C. Hindmarsh, Description and Use of LSODE, the Livermore Solver for Ordinary Differential Equations, Lawrence Livermore National Laboratory Report, NASA Reference Publication, 1993.
[10] K. Subramanyan, Multi-objective optimization of hybrid fuel cell power systems under uncertainty and the value of research, Master's thesis, University of Illinois at Chicago, Chicago, IL, 2004.
[11] U.S. Department of Energy, Fuel Cell Handbook, fifth ed., 2000.
[12] AspenTech, Aspen Plus Documentation, version 12.1, AspenTech, Cambridge, MA, 2003.
[13] R. Geisbrecht, Compact electrochemical reformer based on SOFC technology, in: AIChE Spring National Meeting, Atlanta, GA, 2000.
[14] L. Petruzzi, S. Cocchi, F. Fineschi, A global thermo-electrochemical model for SOFC systems design and engineering, J. Power Sources 118 (2003) 96–107.
[15] P. Aguiar, D. Chadwick, L. Kershenbaum, Modelling of an indirect internal reforming solid oxide fuel cell, Chem. Eng. Sci. 57 (10) (2002) 1665–1677.
[16] S. Campanari, Thermodynamic model and parametric analysis of a tubular SOFC module, J. Power Sources 92 (1–2) (2001) 26–34.
[17] S.H. Chan, K.A. Khor, Z.T. Xia, A complete polarization model of a solid oxide fuel cell and its sensitivity to the change of cell component thickness, J. Power Sources 93 (1–2) (2001) 130–140.
[18] R. Cownden, M. Nahon, M.A. Rosen, Modelling and analysis of a solid polymer fuel cell system for transportation applications, Int. J. Hydrogen Energy 26 (6) (2001) 615–623.
[19] S. Nagata, A. Momma, T. Kato, Y. Kasuga, Numerical analysis of output characteristics of tubular SOFC with internal reformer, J. Power Sources 101 (1) (2001) 60–71.
[20] G. Xui-Mei, K. Hidajat, C. Ching, Simulation of a solid oxide fuel cell for oxidative coupling of methane, Catal. Today 50 (1) (1999) 109–116.
[21] A.V. Virkar, J. Chen, C.W. Tannel, J. Kim, The role of electrode microstructure on activation and concentration polarizations in solid oxide fuel cells, Solid State Ionics 131 (2000) 189–198.
[22] A.M. Al-Qattan, D.J. Chmielewski, S. Al-Hallj, J.R. Selman, A novel design for solid oxide fuel cell stacks, Chem. Eng. Sci. 59 (2004) 131–137.
[23] D.J. Hall, R.G. Colclaser, Transient modeling and simulation of a tubular solid oxide fuel cell, IEEE Trans. Energy Conversion 14 (3) (1999) 749–753.
[24] F. Baratto, Impacts assessment and trade-offs of fuel cell based auxiliary power units, Master's thesis, University of Illinois at Chicago, Chicago, IL, 2004.
[25] Arthur D. Little, Inc., Conceptual Design of POX/SOFC 5 kW net System, Final Report to Department of Energy, National Energy Technology Laboratory, 2001.
[26] T. Tsepin, A.S. Barnett, Effect of LSM–YSZ cathode on thin electrolyte solid oxide fuel cell performance, Solid State Ionics 93 (1997) 207–217.
[27] X. Huang, Z. Liu, Z. Lu, L. Pei, R. Zhu, Y. Liu, J. Miao, Z. Zhang, W. Su, A Ni–YSZ composite containing $Ce_{0.9}Ca_{0.1}O_{2-\delta}$ particles as an anode for SOFCs, J. Phys. Chem. Solids 64 (2003) 2379–2384.
[28] J.H. Lee, J.W. Heo, D.S. Lee, J. Kim, G.H. Kim, H.W. Lee, H.S. Song, J.H. Moon, The impact of anode microstructure on the power generating characteristic of SOFC, Solid State Ionics 158 (2003) 225–232.
[29] R.J. Gorte, H. Kim, J.H. Vohs, Novel SOFC anodes for the direct electrochemical oxidation of hydrocarbon, J. Power Sources 106 (2002) 10–15.
[30] S.P. Jiang, P.J. Callus, S.P.S. Badwal, Fabrication and performance of Ni/3 mol% Y_2O_3–ZrO_2 cermet anodes for solid oxide fuel cells, Solid State Ionics 132 (2000) 1–14.
[31] X. Zhang, S. Ohara, R. Maric, K. Mukai, T. Fukui, H. Yoshida, M. Nishimura, T. Inagaki, K. Miura, Ni–SDC cermet anode for medium temperature solid oxide fuel cell with lanthanum gallate electrolyte, J. Power Sources 83 (1999) 170–177.
[32] X. Huang, Z. Lu, L. Pei, Z. Liu, Y. Liu, R. Zhu, J. Miao, Z. Zhang, W. Su, An anode for solid oxide fuel cells: $NiO + (Ce_{0.9}Ca_{0.1}O_{1.9})_{0.25}(YSZ)_{0.75}$ solid solution, J. Alloys Compd. 360 (2003) 294–297.
[33] J. Koh, Y. Yoo, J. Park, H.C. Lim, Carbon deposition and cell performance of Ni/YSZ anode support SOFC with methane fuel, Solid State Ionics 149 (2002) 157–166.
[34] Z. Lu, L. Pei, T. He, X. Huang, Z. Liu, Y. Ji, X. Zhao, W. Su, Study on new copper containing SOFC anodes, J. Alloys Compd. 334 (2002) 299–303.
[35] T. Hibino, A. Hashimoto, M. Yano, M. Suzuki, M. Sano, Ru-catalyzed anode materials for direct hydrocarbon SOFCs, Electrochem. Acta 48 (2003) 2531–2537.
[36] S.P. Jiang, G. Love, L. Apateanu, Effect of contact between electrode and current collector on the performance of solid oxide fuel cells, Solid State Ionics 160 (2003) 15–26.
[37] S. Hui, A. Petric, Evaluation of yittirium-doped $SrTiO_3$ as an anode for solid oxide fuel cells, J. Eur. Ceramic Soc. 22 (2002) 1673–1681.

[38] J.H. Kim, R.H. Song, K.S. Song, S.H. Syun, D.R. Shin, H. Yokokawa, Fabrication and characteristics of anode-supported flat tube solid oxide fuel cell, J. Power Sources 122 (2003) 138–143.
[39] T. Ingaki, K. Miura, H. Yoshida, R. Maric, S. Ohara, X. Zhang, K. Mukai, T. Fukui, High performance electrodes for reduced temperature solid oxide fuel cell with doped lanthanum gallate electrolyte II. La(Sr)CoO_3 cathode, J. Power Sources 86 (2000) 347–351.
[40] H. Uchida, S. Arisaka, M. Watanabe, High performance electrodes for medium-temperature solid oxide fuel cells: activation of La(Sr)CoO_3 cathode with highly dispersed Pt metal electrocatalysts, Solid State Ionics 135 (2000) 347–351.
[41] C. Xia, M. Liu, Low-temperature SOFCs based on $Gd_{0.1}Ce_{0.9}O_{1.95}$ fabricated by dry pressing, Solid State Ionics 144 (2001) 249–255.
[42] D. Larrain, et al., Thermal modeling of a small anode supported solid oxide fuel cell, J. Power Sources 118 (2003) 367–374.
[43] A. Kaiser, J. Van Herle, R. Marechal, D. Favrat, Tetragonal tungsten bronze type phases $(Sr_{1-x}Ba_x)_{0.6}Ti_{0.2}Nb_{0.8}O_{3-\delta}$: material characterization and performance as SOFC anodes, Solid State Ionics 135 (2000) 519–524.
[44] O.A. Marina, C. Bagger, S. Primdahl, M. Mogensen, A solid oxide fuel cell with gadolinia-doped ceria anode: preparation and performance, Solid State Ionics 123 (1999) 199–208.
[45] S. Wang, Y. Jiang, Y. Zhang, W. Li, J. Yan, Z. Lu, Electrochemical performance of mixed ionic–electronic conducting oxides as anodes for solid oxide fuel cell, Solid State Ionics 120 (1999) 75–84.
[46] N.T. Hart, N.P. Brandon, M.J. Day, N.L. Rey, Functionally graded composite cathodes for solid oxide fuel cells, J. Power Sources 106 (2002) 42–50.
[47] H.S. Yoon, S.W. Choi, D. Lee, B.H. Kim, Synthesis and characterization of $Gd_{1-x}Sr_xMnO_3$ cathode for solid oxide fuel cells, J. Power Sources 93 (2001) 1–7.
[48] T. Tsai, S.A. Barnett, Effect of LSM–YSZ cathode on thin-electrolyte solid oxide fuel cell performance, Solid State Ionics 93 (1997) 207–217.
[49] T. Kenjo, Y. Kanehira, Influence of the local variation of the polarization resistance on SOFC cathodes, Solid State Ionics 148 (2002) 1–14.
[50] S.P. Yoon, J. Han, S.W. Nam, T.H. Lim, I.H. Oh, S.A. Hong, Y.S. Yoo, H.C. Lim, Performance of anode-supported solid oxide fuel cell with $La_{0.85}Sr_{0.15}MnO_3$ cathode modified by sol–gel coating technique, J. Power Sources 106 (2002) 160–166.
[51] H. Taherparvar, K.J. Kilner, R.T. Baker, M. Sahibzada, Effect of humidification at anode and cathode in proton-conducting SOFCs, Solid State Ionics 162–163 (2003) 297–303.
[52] J. Van Herle, R. Ihringer, R.V. Cavieres, L. Constantin, O. Bucheli, Anode supported solid oxide fuel cells with screen printed cathodes, J. Eur. Ceramic Soc. 21 (2001) 1855–1859.
[53] K. Kuroda, I. Hashimoto, K. Adachi, J. Akikusa, Y. Tamou, N. Komada, T. Ishihara, Y. Takita, Characterization of solid oxide fuel cell using doped lanthanum gallate, Solid State Ionics 132 (2000) 199–208.
[54] M. Sahibzada, B. Steele, K. Zheng, R. Rudkin, I.S. Metcalfe, Development of solid oxide fuel cell based on Ce(Gd)O_{2-x} electrolyte film for intermediate temperature operation, Catal. Today 38 (1997) 459–466.
[55] T. Ishihara, T. Shibayama, S. Ishikawa, K. Hosoi, H. Nishiguchi, Y. Takita, Novel fast oxide ion conductor and application for the electrolyte of solid oxide fuel cell, J. Eur. Ceramic Soc. (2003).
[56] N. Maffei, A.K. Kuriakose, Solid oxide fuel cells of ceria doped with gadolinium and praseodymium, Solid State Ionics 107 (1998) 67–71.
[57] M. Sahibzada, B.C.H. Steele, D. Barth, R.Z. Rudkin, I.S. Metcalfe, Operation of solid oxide fuel cells at reduced temperatures, Fuel 78 (1999) 639–643.
[58] T. Fukui, Performance of intermediate temperature solid oxide fuel cells with La(Sr)Ga(Mg)O_3 electrolyte film, J. Power Sources 106 (2002) 142–145.
[59] N. Maffei, A.K. Kuriakose, Performance of planar single cell lanthanum gallate based solid-oxide fuel cells, J. Power Sources 75 (1998) 162–166.
[60] H. Ohrui, Performance of a solid oxide fuel cell fabricated by co-firing, J. Power Sources 71 (1998) 185–189.
[61] S. Wang, T. Kato, S. Nagata, T. Kaneko, N. Iwashita, T. Honda, M. Dokiya, Electrodes and performance analysis of a ceria electrolyte SOFC, Solid State Ionics 152–153 (2002) 477–484.
[62] K. Huang, J.B. Goodenough, A solid oxide fuel cell based on Sr- and Mg-doped $LaGaO_3$ electrolyte: the role of a rare-earth oxide buffer, J. Alloys Compd. 303–304 (2000) 454–464.
[63] H. He, X. Huang, L. Chen, Sr-doped $LaInO_3$ and it's possible application in a single layer SOFC, Solid State Ionics 130 (2000) 183–193.
[64] S. Taniguchi, M. Kadowaki, T. Yasuo, Y. Akiyama, Y. Miyake, K. Nishio, Improvement of thermal cycle characteristics of a planar-type solid oxide fuel cell by using ceramic fiber as sealing material, J. Power Sources 90 (2000) 163–169.
[65] P. Charpentier, P. Fragnaud, D.M. Schleich, E. Gehain, Preparation of thin film SOFCs working at reduced temperature, Solid State Ionics 135 (2000) 373–380.
[66] B. Zhu, X.T. Yang, J. Xu, Z.G. Zhu, S.J. Ji, M.T. Sun, J.C. Sun, Innovative low temperature SOFCs and advanced materials, J. Power Sources 118 (2003) 47–53.
[67] C. Hatchwell, N.M. Sammes, I.W.M. Brown, Fabrication and properties of $Ce_{0.8}Gd_{0.2}O_{1.9}$ electrolyte-based tubular solid oxide fuel cells, Solid State Ionics 126 (1999) 201–208.
[68] S.P.S. Badwal, F.T. Ciacchi, D. Milosevic, Scandia–zirconia electrolytes for intermediate temperature solid oxide fuel cell operation, Solid State Ionics 136–137 (2000) 91–99.
[69] S. De Souza, S.J. Visco, L.C. De Jonghe, Thin film solid oxide fuel cell with high performance at low temperature, Solid State Ionics 98 (1997) 57–61.
[70] J. Padulles, G.W. Ault, J.R. McDonald, An integrated SOFC plant dynamic model for power systems simulation, J. Power Sources 86 (2000) 495–500.
[71] U. Diwekar, Manual for the Hammersely Sequence Sampling, 2000.
[72] U.M. Diwekar, Introduction to Applied Optimization, Kluwer Academic Publishers, Dordrecht, Netherlands, 2003.
[73] F. Huiling, et al., The apparent kinetics of H_2S removal by zinc oxide in the presence of hydrogen, Fuel 81 (2002) 91–96.
[74] P. Yrjas, K. Lisa, M. Hupa, Limestone and dolomite as sulfur absorbents under pressurized gasification conditions, Fuel 75 (1997) 89–95.
[75] M. Pineda, J.M. Palacios, E. Garcia, C. Cilleruelo, J.V. Iberra, Modeling of performance of zinc ferrites as high-temperature desulfurizing sorbents in a fixed-bed reactor, Fuel 76 (1997) 567–573.
[76] Y. Yoon, M.W. Kim, Y.S. Yoon, S.H. Kim, A kinetic study on medium temperature desulfurization using a natural manganese ore, Chem. Eng. Sci. 58 (2003) 2079–2087.
[77] L. Fenouil, S. Lynn, Design of entrained-flow and moving-, packed-, and fluidized-bed sorption systems: grain-model kinetics for hot coal-gas desulfurization with limestone, Ind. Eng. Chem. Res. 35 (1996) 1024–1043.
[78] J. Adanez, L.F. De Diego, F.G. Labiano, A. Abad, Kinetics of H_2S based reaction with calcined calcium-based sorbents, Energy Fuels 12 (1998) 617–625.
[79] E. Garcia, K. Cilleruelo, J.V. Ibarra, M. Pineda, J.M. Palacios, Kinetic study of high-temperature removal of H_2S by novel metal oxide sorbents, Ind. Eng. Chem. Res. 36 (1997) 846–853.
[80] J. Abbasian, R.B. Slimane, A regenerable copper-based sorbent for H_2S removal from coal gases, Ind. Eng. Chem. Res. 37 (1998) 2775–2782.
[81] M. Hartman, K. Svoboda, O. Trnka, Ji. Cermak, Reaction between hydrogen sulfide and limestone calcines, Ind. Eng. Chem. Res. 41 (2002) 2392–2398.

[82] S. Yasyerli, G. Dogu, I. Ar, Activities of copper oxide and Cu–V and Cu–Mo mixed oxides for H_2S removal in the presence and absence of hydrogen predictions of a deactivation model, Ind. Eng. Chem. Res. 40 (2001) 5206–5214.
[83] Z. Li, et al., Cu–Cr–O and Cu–Ce–O regenerable oxide sorbents for hot gas desulfurization, Ind. Eng. Chem. Res. 36 (1997) 187–196.
[84] L. Fenouil, M.F. Stephanopoulous, Study of calcium-based sorbents for high-temperature H_2S removal. 1. Kinetics of H_2S sorption by uncalcined limestone, Ind. Eng. Chem. Res. 34 (1995) 2324–2333.
[85] W. Bakker, F. Kapteijn, J.A. Moulijn, A high-capacity manganese-based sorbent for regenerative high temperature desulfurization with direct sulfur production: conceptual process application to coal gas cleaning, Chem. Eng. J. 96 (2003) 223–235.
[86] J. Adanez, Labiano F.G., L.F. de Diego, V. Vierro, Utilization of calcium acetate and calcium magnesium acetate for H_2S removal in coal gas cleaning at high temperatures, Energy Fuels 13 (1999) 440–448.
[87] J. Adanez, F.G. Labiano, L.F. de Diego, V. Vierro, H_2S removal in entrained flow reactors by injection of Ca-based sorbents at high temperatures, Energy Fuels 12 (1998) 726–733.
[88] K. Qiu, O. Lindqvist, T. Mattison, Regeneration of calcium sulfide under alternating oxidizing and inert conditions: kinetics and mechanism, Ind. Eng. Chem. Res. 37 (1998) 923–928.